The Astrophysical Journal Letters, 993:L37 (14pp), 2025 November 1 https://doi.org/10.3847/2041-8213/ae146b

The Redshift Distribution of Einstein Probe Transients Supports Their Relation to Gamma-Ray Bursts

Brendan O'Connor[1,12], Paz Beniamini[2,3,4], Eleonora Troja[5], Malte Busmann[6,13], Simone Dichiara[7], Ramandeep Gill[3,8], Jonathan Granot[2,3,4], Michael J. Moss[9], Xander J. Hall[1], Antonella Palmese[1], Niccolò Passaleva[10,11], and Yu-Han Yang[10]
[1] McWilliams Center for Cosmology and Astrophysics, Department of Physics, Carnegie Mellon University, Pittsburgh, PA 15213, USA; boconno2@andrew.cmu.edu
[2] Department of Natural Sciences, The Open University of Israel, P.O Box 808, Ra'anana 4353701, Israel
[3] Astrophysics Research Center of the Open university (ARCO), The Open University of Israel, P.O Box 808, Ra'anana 4353701, Israel
[4] Department of Physics, The George Washington University, Washington, DC 20052, USA
[5] Department of Physics, University of Rome "Tor Vergata," via della Ricerca Scientifica 1, I-00133 Rome, Italy
[6] University Observatory, Faculty of Physics, Ludwig-Maximilians-Universität München, Scheinerstr. 1, 81679 Munich, Germany
[7] Department of Astronomy and Astrophysics, The Pennsylvania State University, 525 Davey Lab, University Park, PA 16802, USA
[8] Instituto de Radioastronomía y Astrofísica, Universidad Nacional Autónoma de México, Antigua Carretera a Pátzcuaro # 8701, Ex-Hda. San José de la Huerta, Morelia, Michoacán, C.P. 58089, México
[9] NASA Postdoctoral Program Fellow, NASA Goddard Space Flight Center, Greenbelt, MD 20771, USA
[10] Dipartimento di Fisica, Università di Tor Vergata, Via della Ricerca Scientifica, 1, 00133 Rome, Italy
[11] Dipartimento di Fisica, Università di Roma "La Sapienza," Ple Aldo Moro, 2, 00185 Rome, Italy
Received 2025 September 8; revised 2025 October 13; accepted 2025 October 13; published 2025 October 31

Abstract

The launch of the Einstein Probe unleashed a new era of high-energy transient discovery in the largely unexplored soft X-ray band. The Einstein Probe has detected a significant number of fast X-ray transients that display no gamma-ray emission, complicating their robust association with more common gamma-ray bursts. To explore their possible connection, we analyzed the redshift distribution of both Einstein Probe fast X-ray transients and long-duration gamma-ray bursts. A comparative analysis of their cumulative redshift distributions using nonparametric two-sample tests, namely the Kolmogorov–Smirnov and Anderson–Darling tests, finds no statistically significant difference. These tests favor that their redshifts are drawn from the same underlying distribution. This empirical connection between Einstein Probe transients and long gamma-ray bursts is further supported by their agreement with the so-called "Amati relation" between the spectral peak energy and the isotropic-equivalent energy. Together, these results indicate that most extragalactic Einstein Probe fast X-ray transients are closely related to long gamma-ray bursts and originate from a massive star (collapsar) progenitor channel. Our findings highlight the role of the Einstein Probe in uncovering the missing population of failed jets and dirty fireballs that emit primarily at soft X-ray wavelengths.

Unified Astronomy Thesaurus concepts: X-ray astronomy (1810); X-ray transient sources (1852); Gamma-ray bursts (629)

1. Introduction

The high-energy transient sky has historically been dominated by long-duration gamma-ray bursts (GRBs; C. Kouveliotou et al. 1993), which are detected at an observed rate of approximately one per day. These powerful explosions are linked to the deaths of massive stars (e.g., collapsars; S. E. Woosley 1993; A. I. MacFadyen & S. E. Woosley 1999), which launch highly collimated, ultrarelativistic jets (D. A. Frail et al. 1997). The resulting emission is detectable across the electromagnetic spectrum, from gamma-ray to radio wavelengths (R. Sari et al. 1998; R. A. M. J. Wijers & T. J. Galama 1999; J. Granot & R. Sari 2002).

The launch of the Einstein Probe (EP; W. Yuan et al. 2015, 2022; W. Yuan et al. 2025) has seen a sharp rise in the discovery rate of fast X-ray transients. The majority of these high-energy transients do not display any gamma-ray emission, while a handful have been solidly associated with GRBs (Y. H. I. Yin et al. 2024; Y. Liu et al. 2025). As such, the exact nature of the majority of the EP transient population, as well as their relation to the deaths of massive stars, is uncertain. While the broad class of fast X-ray transients displays a great diversity in their properties (J. A. Quirola-Vásquez et al. 2022, 2023), the fast transients discovered by EP, even those without prompt gamma-ray detections, tend to show GRB-like afterglow properties and energetics (H. Sun et al. 2025; Y. H. I. Yin et al. 2024; M. Busmann et al. 2025; S.-Q. Jiang et al. 2025b; Y. Liu et al. 2025; R. Ricci et al. 2025; M. Yadav et al. 2025). Additionally, a number of nearby EP transients have been associated with Type Ic-BL supernovae (J. C. Rastinejad et al. 2025; G. P. Srinivasaragavan et al. 2025a; S. Srivastav et al. 2025; J. N. D. van Dalen et al. 2025), typical of those found to follow long GRBs (S. E. Woosley & J. S. Bloom 2006). Altogether, there are multiple lines of evidence that strongly suggest that many EP transients are related to GRBs, or at least come from similar progenitors.

In this work, we utilize the observed redshift distribution of EP-detected fast X-ray transients to probe their connection to

[12] McWilliams Fellow.
[13] Recipient of a Wübben Stiftung Wissenschaft Student Grant.

long-duration GRBs. The redshift distribution of a class of astrophysical transients imprints key information on their origins, including their connection to star formation. We find that properties of EP transients, including their overall redshifts and energetics, align closely with long GRBs, supporting their association with the core collapse deaths of massive stars.

Throughout the manuscript we adopt a standard ΛCDM cosmology (Planck Collaboration et al. 2020) with $H_0 = 67.4\,\mathrm{km\,s^{-1}\,Mpc^{-1}}$, $\Omega_m = 0.315$, and $\Omega_\Lambda = 0.685$.

2. Source Sample and Observations

2.1. Sample of Einstein Probe Transients

EP is a new soft X-ray mission (W. Yuan et al. 2015, 2022; W. Yuan et al. 2025) with wide-field capabilities. EP was launched on 2024 January 9 and is currently surveying the sky in the soft X-ray band between 0.5 and 4.0 keV. The Wide-field X-ray Telescope (WXT) has an instantaneous field of view (FOV) of 3600 $\mathrm{deg^2}$ and is capable of autonomously detecting transients on board the spacecraft (W. Yuan et al. 2025; X. Zhao et al. 2025). These EP/WXT transients are then generally reported through General Coordinate Network (GCN) Notices[14] and, later, GCN Circulars.[15] The delay of these reports from the EP/WXT trigger time varies from event to event based on the data's downlink latency, among other factors.

Due to the low energy range (0.5–4.0 keV) observed by WXT, flaring stars are a major source of contamination that must be filtered out to select a clean extragalactic sample of EP transients. These contaminant sources are not provided a standard EP designation (i.e., EPYYMMDDa) and are instead labeled by their trigger identification number (i.e., EP#XXXXXXXXXXX). In order to avoid further contamination from Galactic sources, EP/WXT's on-board trigger algorithm does not relay alerts for transients lying at close proximity to the Galactic plane (e.g., EP250702a; H. Q. Cheng et al. 2025).

After removing these contaminating sources, the rate of extragalactic EP transients is ∼70–80 per year. As of 2025 August 29, we find ∼113 publicly reported EP/WXT transients fitting this criterion. While the information publicly reported by EP varies from event to event, in general the available quantities communicated based on the WXT trigger are source localization, approximate duration, soft X-ray photon index, time-averaged (unabsorbed) flux, and, in some cases, the peak X-ray flux. Usually there is additional information based on observations with the Follow-up X-ray Telescope (FXT; Y. Chen et al. 2025; J. Zhang et al. 2025), if it is available. In Table 1, we compile the available photon index and flux information on a per-event basis for events in our sample, which is further described below.

2.2. Compilation of the Einstein Probe Redshift Distribution

We have compiled a sample of redshifts for EP/WXT transients reported publicly in GCN Circulars or available in the published literature (including the spectra reported in Appendix A; Figure A1). Our sample comprises all publicly reported EP sources up to 2025 August 29. In total, we find ∼113 publicly reported EP/WXT transients. Of these EP sources, we find 26 with secure spectroscopic redshifts. The redshift completeness is therefore only ∼23%. The catalog of EP sources with redshifts is tabulated in Table 1.

The majority of these redshifts are determined through the identification of absorption lines detected in optical spectroscopy, with the exception of a handful that are based on their association with a host galaxy (from the detection of underlying emission lines). The measure of absorption lines provides a robust lower limit to the redshift, which is generally assumed to be the precise redshift of the transient. While the detection of emission lines provides an accurate redshift for a given galaxy, there is always the possibility that the galaxy association is due to a (either foreground or background) chance alignment (J. S. Bloom et al. 2002). As such, this handful of EP transient redshifts is less secure (see Appendix B for further discussion).

2.3. Redshift and Optical Afterglow Completeness

The redshift completeness for EP transients is lower than the completeness for Swift GRBs (e.g., J. Hjorth et al. 2012; P. Jakobsson et al. 2012; D. A. Perley et al. 2016; J. Selsing et al. 2019). However, whereas Swift is equipped with the Ultra-Violet Optical Telescope (UVOT; P. W. A. Roming et al. 2005) for rapid optical follow-up, EP has to rely on ground-based follow-up, which introduces a delay in the discovery and characterization of the optical counterpart.

Here we discuss the impact of latency on the optical afterglow and redshift completeness. We retrieved the GCN Notice[16] time and EP trigger time from the Astro-COLIBRI[17] platform (P. Reichherzer et al. 2021). These values are available starting in 2024 July for 93 EP transients, which misses only the first 4–5 months of the commissioning phase of EP. We therefore only lack this information for 18 out of 113 EP sources. Only 2 out of these 18 sources have redshifts (EP240315a and EP240414a). Therefore, we consider the completeness of EP transients using the 24 redshifts (out of 93[18] events) uncovered after 2024 July, which yields a similar redshift completeness of ∼25%. Figure 1 shows the reporting latency (defined as the delay between the on-board trigger and public notice to the community) of EP transients.

For those reported within 12 hr, we find that 21 out of 60 have a measured redshift (∼35%). Shortening the delay to those reported through low-latency GCN Notice within 3 hr, we find that 15 out of 32, i.e., ∼47%, have a measured redshift, nearly a factor of 2 increase to the full sample when not accounting for reporting delay. Of the 26 (27% of EP transients) reported publicly within 1 hr of discovery, 13 (50%) have a measured redshift.

This shows that reporting latency is an important factor in the discovery of optical afterglows (see also A. Aryan et al. 2025) and therefore spectroscopic redshift measurements. We suggest that this delay has a major (artificial) impact on the optical afterglow completeness and is large compared to Swift GRBs. This discrepancy in completeness is due to the combination of a few factors, including (i) the shorter delay

[14] https://gcn.nasa.gov/notices
[15] https://gcn.nasa.gov/circulars
[16] A GCN Notice is a low-latency, machine readable alert and differs from human readable GCN circulars that are generally sent on longer timescales across all ingested missions.
[17] https://astro-colibri.com/
[18] We note that this does not include the handful of EP events reported through GCN Circulars (and not reported through any GCN Notice) with longer delays (e.g., EP250827b) and only includes those with a GCN Notice.

Table 1
Catalog of EP Sources Used in This Work

Name	Redshift	GRB?	$\Gamma_{\rm WXT}$	$F_{\rm WXT,avg}$ (erg cm^{-2} s^{-1})	$F_{\rm WXT,peak}$ (erg cm^{-2} s^{-1})	References
EP240315a	4.859	GRB 240315C	1.4 ± 0.1	$(5.3^{+1.0}_{-0.7}) \times 10^{-10}$	$(4.6^{+0.8}_{-0.7}) \times 10^{-9}$	(1, 2, 3)
EP240414a	0.401	⋯	$3.1^{+0.7}_{-0.8}$	$(6.5^{+1.3}_{-1.0}) \times 10^{-10}$	$(2.2 \pm 0.7) \times 10^{-9}$	(4, 5, 6)
EP240801a	1.673	XRF 240801B	1.99 ± 0.18	$(4.8 \pm 3.1) \times 10^{-10}$	$(1.2^{+0.6}_{-0.8}) \times 10^{-8}$	(7, 8, 9, 10)
EP240804a	3.662	GRB 240804B	$0.7^{+1.2}_{-0.4}$	$(6.1^{+2.6}_{-1.6}) \times 10^{-10}$	⋯	(11, 12, 13)
EP240806a	2.818	⋯	$2.6^{+1.2}_{-1.0}$	$(1.9^{+1.8}_{-0.6}) \times 10^{-9}$	⋯	(15, 16)
EP241021a	0.748	⋯	1.8 ± 0.6	$(3.31^{+0.13}_{-0.09}) \times 10^{-10}$	1.0×10^{-9}	(16, 17, 18)
EP241030a[a]	1.411	GRB 241030A	$2.5^{+0.8}_{-0.7}$	$(7.5^{+3.0}_{-2.4}) \times 10^{-11}$	⋯	(19, 20, 21)
EP241107a	0.456	⋯	⋯	⋯	4.2×10^{-9}	(22, 23)
EP241113a	1.53	⋯	1.3 ± 0.2	$(5.57^{+1.26}_{-0.76}) \times 10^{-10}$	⋯	(24, 25)
EP241217a	4.59	⋯	$1.9^{+0.7}_{-0.6}$	$(7.3 \pm 0.3) \times 10^{-10}$	⋯	(26, 27)
EP241217b	1.879	GRB 241217A	$1.57^{+0.22}_{-0.21}$	$(1.19 \pm 0.10) \times 10^{-9}$	⋯	(28, 29, 30)
EP250108a	0.176	⋯	2.8 ± 1.1	$(6.4^{+22.5}_{-3.0}) \times 10^{-11}$	$(1.80^{+0.20}_{-0.06}) \times 10^{-10}$	(31, 32, 33, 34)
EP250125a	2.89	⋯	0.8 ± 0.5	$(1.8^{+0.7}_{-0.5}) \times 10^{-9}$	⋯	(35, 36)
EP250205a	3.55	GRB 250205A	$2.5^{+1.7}_{-1.2}$	$(4.2 \pm 1.1) \times 10^{-10}$	⋯	(37, 38, 39)
EP250215a	4.61	GRB 250215A	⋯	⋯	⋯	(40, 41, 42)
EP250223a	2.756	⋯	2.1 ± 0.6	$(4.4^{+1.4}_{-1.1}) \times 10^{-10}$	2.0×10^{-9}	(43, 44)
EP250226a	3.315	GRB 250226A	⋯	⋯	9.8×10^{-9}	(45, 46, 47)
EP250302a	1.131	⋯	0.6 ± 0.4	$(7.0^{+2.0}_{-1.6}) \times 10^{-9}$	9.0×10^{-9}	(48, 49)
EP250304a	0.200	⋯	2.2 ± 0.1	$(5.3^{+0.4}_{-0.4}) \times 10^{-10}$	⋯	(50, 51)
EP250321a	4.368	⋯	0.66 ± 0.17	$(1.73^{+0.21}_{-0.19}) \times 10^{-9}$	4.2×10^{-9}	(52, 53)
EP250404a	1.88	GRB 250404A	$0.41^{+0.26}_{-0.28}$	$(5.9^{+2.2}_{-1.6}) \times 10^{-8}$	⋯	(54, 55, 56, 57)
EP250416a	0.963	GRB 250416C	$0.32^{+1.00}_{-0.78}$	$(5.66 \pm 1.77) \times 10^{-9}$	$(1.9 \pm 0.8) \times 10^{-8}$	(58, 59, 60)
EP250427a	1.52	GRB 250427A	$1.70^{+0.36}_{-0.34}$	$(1.96^{+0.31}_{-0.23}) \times 10^{-9}$	2.0×10^{-8}	(61, 62, 63, 64)
EP250704a[b]	0.661	GRB 250704B	1.7 ± 1.3	$(1.3^{+0.8}_{-1.1}) \times 10^{-9}$	6.0×10^{-7}	(65, 66, 67)
EP250821a	0.577	⋯	1.2 ± 0.5	$(1.3 \pm 0.4) \times 10^{-9}$	⋯	(68, 69, 70)
EP250827a	1.61	⋯	$0.73^{+0.50}_{-0.47}$	$(1.71^{+0.42}_{-0.34}) \times 10^{-9}$	⋯	(71, 72, 73)

Notes.
[a] EP241030a is likely the afterglow of GRB 241030A and not the prompt emission (H. Z. Wu et al. 2024).
[b] EP250704a is associated with the short-duration GRB 250704B (D. Frederiks et al. 2025b).
References. The WXT properties including X-ray photon index $\Gamma_{\rm WXT}$ and peak and time-averaged X-ray flux are reported. The X-ray fluxes are in the 0.5–4 keV band. (1) Y. Liu et al. (2025); (2) A. J. Levan et al. (2024a); (3) A. Saccardi et al. (2024); (4) H. Sun et al. (2025); (5) J. N. D. van Dalen et al. (2025); (6) S. Srivastav et al. (2025); (7) S.-Q. Jiang et al. (2025b); (8) H. Zhou et al. (2024a); (9) J. A. Quirola-Vásquez et al. (2024c); (10) W. Zheng et al. (2024a); (11) Y. Wang et al. (2024); (12) D. Frederiks et al. (2024); (13) A. Bochenek et al. (2024); (14) Q. Y. Wu et al. (2024); (15) J. A. Quirola-Vásquez et al. (2024a); (16) X. Shu et al. (2025); (17) I. Pérez-Fournon et al. (2024); (18) G. Pugliese et al. (2024); (19) H. Z. Wu et al. (2024); (20) N. J. Klingler et al. (2024); (21) W. Zheng et al. (2024b); (22) R. Z. Li et al. (2024); (23) J. A. Quirola-Vásquez et al. (2025); (24) Z. Y. Liu et al. (2024); (25) J. A. Quirola-Vásquez et al. (2024b); (26) H. Zhou et al. (2024b); (27) A. J. Levan et al. (2024b); (28) H. Zhou et al. (2024c); (29) B. Marius et al. (2024); (30) B. Schneider et al. (2024); (31) W. X. Li et al. (2025); (32) J. C. Rastinejad et al. (2025); (33) R. A. J. Eyles-Ferris et al. (2025); (34) G. P. Srinivasaragavan et al. (2025b); (35) Q. Y. Wu et al. (2025); (36) A. J. Levan et al. (2025d); (37) Z. Y. Liu et al. (2025); (38) A. Saccardi et al. (2025b); (39) A. de Ugarte Postigo et al. (2025); (40) C. Y. Wang et al. (2025); (41) Fermi GBM Team (2025a); (42) R. Sanchez-Ramirez et al. (2025); (43) Y. Wang et al. (2025b); (44) A. J. Levan et al. (2025a); (45) S.-Q. Jiang et al. (2025a); (46) Fermi GBM Team (2025b); (47) Z. P. Zhu et al. (2025a); (48) C. Y. Dai et al. (2025); (49) L. Izzo et al. (2025a); (50) Y. J. Zhang et al. (2025); (51) A. Saccardi et al. (2025c); (52) D. F. Hu et al. (2025); (53) Z. P. Zhu et al. (2025b); (54) Y. H. I. Yin et al. (2025b); (55) D. Frederiks et al. (2025a); (56) Y. H. I. Yin et al. (2025a); (57) R. Z. Li et al. (2025); (58) H. Zhou et al. (2025); (59) D. Svinkin et al. (2025); (60) A. J. Levan et al. (2025c); (61) Y. Wang et al. (2025a); (62) M. E. Ravasio et al. (2025); (63) R. Chornock et al. (2025); (64) A. Saccardi et al. (2025a); (65) A. Li et al. (2025); (66) D. Frederiks et al. (2025b); (67) J. An et al. (2025b); (68) Y. F. Liang et al. (2025); (69) J. An et al. (2025a); (70) B. O'Connor et al. (2025b); (71) K. R. Ni et al. (2025); (72) A. J. Levan et al. (2025e); (73) N. Passaleva et al. (2025).

(<1 minute) in public notice for Swift,[19] (ii) the shorter delay in acquiring arcsecond-precision positions with the Neil Gehrels Swift Observatory (N. Gehrels et al. 2004) X-ray Telescope (XRT; D. N. Burrows et al. 2005), and (iii) the lack of initial imaging with Swift UVOT that allows for rapid spectroscopy with a knowledge of the optical brightness. While the prompt gamma-ray localizations of the Swift Burst Alert Telescope (BAT; S. D. Barthelmy et al. 2005) are comparable to the WXT localization, the XRT and UVOT localizations are significantly more accurate and avoid necessary image scanning over a multiarcminute field. This aids in the rapid identification of the optical counterpart, increasing the likelihood of spectroscopy (e.g., J. Selsing et al. 2019). We note that Swift performs rapid Priority 0 (P0; see A. Tohuvavohu et al. 2024) target of opportunity (ToO) observations[20] for EP transients reported in near real time ($\leqslant$4 hr latency; J. Kennea 2025, private communication), which can provide a more rapid, precise localization of the X-ray source. This may be a factor in the increasing redshift completeness for EP transients reported in lower latency.

As there is no intrinsic difference in a source with a longer or shorter latency in reporting its discovery, we consider that

[19] https://gcn.nasa.gov/missions/swift

[20] https://www.swift.ac.uk/EP/

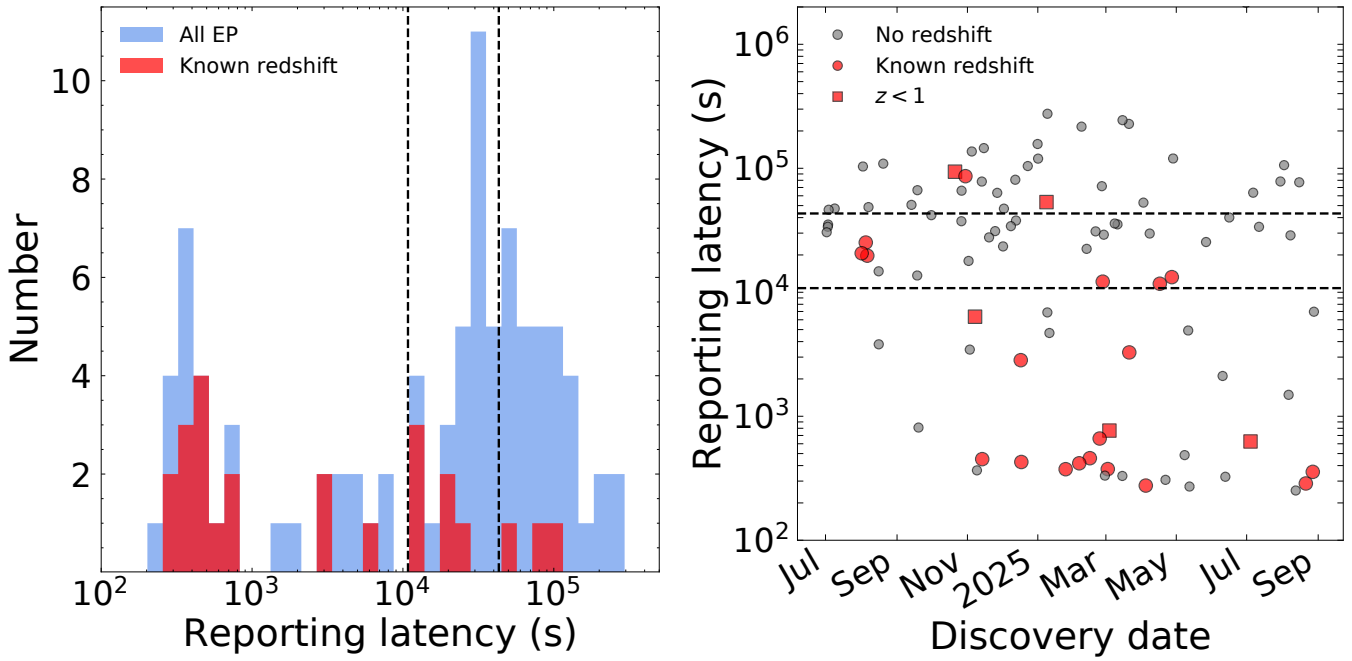

Figure 1. Left: histogram of the EP reporting latency measured as the time between GCN notice and EP trigger time. All EP transients (from 2024 July onward) are shown in blue, and those with measured redshifts are marked in red. The dashed lines mark 3 and 12 hr from the EP trigger. Right: reporting latency versus discovery date for EP transients. Those with no redshift are marked in gray, and those with redshifts are marked in red. Sources with redshift at $z < 1$ are shown by squares.

this does not have a large impact on our results or interpretation. In fact, it supports our overall conclusion by showing that the low-redshift completeness of EP transients is not necessarily an intrinsic property. While it has been proposed that some EP fast X-ray transients are related to "dark" GRBs (A. J. van der Horst et al. 2009) based on their faint optical brightness at a few days after detection (A. Aryan et al. 2025), a comprehensive analysis is required to determine whether this fraction of possible "dark" events is consistent with the fraction observed in GRBs or substantially different. A full investigation of optical darkness in the EP transient population and the optical afterglow completeness of EP fast X-ray transients will be presented in M. Busmann et al. (2025, in preparation).

2.4. Prompt Gamma-Ray Properties

We can break down the sample of EP transients into two additional classes, which we consider separately throughout this manuscript. The first is EP-GRBs, being those with gamma-ray detections from other high-energy monitors. The second are EP transients without gamma-ray detections, which can be referred to as gamma-ray dark events (M. Yadav et al. 2025). As such, there are three samples of EP events (all those with redshift, those with redshift and gamma rays, and those with redshift and without gamma rays) that we consider separately in the analysis presented in Section 3.

Of the sample of EP sources with redshifts (Table 1), 12 events (46% of the sample) were also detected as GRBs (referred to as EP-GRBs throughout this work). The coincident gamma-ray emission detected from these sources displays long durations (>2 s), with the exception of the short burst EP250704a/GRB 250704B (D. Frederiks et al. 2025b; A. Li et al. 2025). While the majority of EP-GRBs triggered high-energy gamma-ray monitors as standard GRBs, some were subthreshold detections based on targeted searches. These include EP240315a/GRB 240315C (Y. Liu et al. 2025), EP240801a/XRF 240801B (S.-Q. Jiang et al. 2025b), and EP250427a/GRB 250427A (M. E. Ravasio et al. 2025). In the case of EP241217b/GRB 241217A, while the gamma-ray emission was first detected (B. Marius et al. 2024) by the Space-based multi-band astronomical Variable Objects Monitor (SVOM; J. Wei et al. 2016), a subthreshold detection (M. E. Ravasio et al. 2024) was made by the Fermi Gamma-ray Space Telescope Gamma-ray Burst Monitor (GBM; C. Meegan et al. 2009). This highlights that limited gamma-ray sensitivity can be a factor in detecting the prompt emission.

While in the majority of cases EP has clearly detected the prompt emission of the transient, we note that EP241030a is very likely a detection of the afterglow of GRB 241030A and not the prompt emission (H. Z. Wu et al. 2024). However, as this still represents an onboard EP/WXT detection (independent of the GRB trigger), we include this transient in our sample of redshifts. This may also be the case for EP250205a/GRB 250205A (A. Saccardi et al. 2025b), as EP detected the emission 410 s (90 s in rest frame) after the gamma-ray trigger due to Earth occultation (Z. Y. Liu et al. 2025). However, a full analysis of the available data is required to robustly make this determination on a case-by-case basis (as for, e.g., EP250404a/GRB 250404A; Y. H. I. Yin et al. 2025a), especially as many joint EP-GRB detections have demonstrated significantly longer duration soft X-ray emission (see, e.g., Y. H. I. Yin et al. 2024, 2025a; Y. Liu et al. 2025).

3. Analysis and Results

3.1. High-energy Properties

While EP/WXT transients clearly display prompt X-ray emission, the majority do not trigger other high-energy hard X-ray or gamma-ray monitors. This can be due to a combination of the low peak energy of their prompt emission spectrum (e.g., EP240414a, EP240801a, EP250108a;

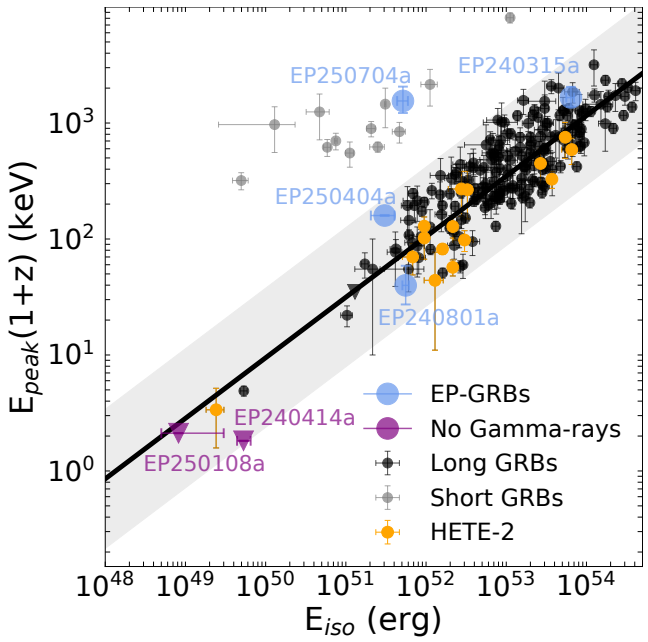

Figure 2. The E_p–$E_{\rm iso}$ plane of GRBs, with short GRBs shown in gray and long GRBs in black. EP transients with gamma-ray detections are shown in blue, and those without gamma rays are shown in purple, with upper limits represented by downward-pointing triangles. We explicitly highlight HETE-2 bursts in orange (A. Pélangeon et al. 2008). The solid black line and 3σ scatter to the correlation for long GRBs are reproduced from L. Amati et al. (2019). The figure is reproduced from S. Dichiara et al. (2021).

S.-Q. Jiang et al. 2025b; W. X. Li et al. 2025; Y. Liu et al. 2025), or the worse sensitivity of gamma-ray detectors compared to EP. Some events that do not trigger on board the gamma-ray spacecraft have been identified as GRBs later in subthreshold searches, such as EP240219a/GRB 240219A (Y. H. I. Yin et al. 2024), EP240315a/GRB 240315C (Y. Liu et al. 2025), and EP240801a/XRF 240801B (S.-Q. Jiang et al. 2025b). It is therefore possible that other EP sources also emit faint gamma rays that cannot be detected to the available gamma-ray sensitivity limits (usually 10–100 times less sensitive than EP/WXT). In Figure 2, we show the standard GRB correlation (e.g., L. Amati et al. 2002; L. Amati 2006) between the rest-frame peak energy $E_p(1+z)$ and the isotropic equivalent gamma-ray energy $E_{\rm iso}$ in the 1–10,000 keV energy range. The sample of long GRBs shown is the same as that used in L. Amati et al. (2008, 2009) and spans multiple missions, including Swift, Fermi, Konus-Wind, BATSE, BeppoSAX, and HETE-2. It has been updated to include the latest results from Fermi (S. Poolakkil et al. 2021) and Konus-Wind (A. Tsvetkova et al. 2017). While only a handful of EP-GRBs have peak energies publicly reported in the literature (S.-Q. Jiang et al. 2025b; W. X. Li et al. 2025; Y. Liu et al. 2025; Y. H. I. Yin et al. 2025a), those that do clearly follow the E_p–$E_{\rm iso}$ plane and show an extension at the faint end of the $E_{\rm iso}$ distribution. This is similar to the conclusion drawn from early intrinsic X-ray flash (XRF) detections (i.e., XRF 020903) by HETE-2 (T. Sakamoto et al. 2004). The clear exception for EP-GRBs in Figure 2 is the location of EP250704a/GRB 250704B (D. Frederiks et al. 2025b), which, combined with its short gamma-ray duration ($\ll$2 s), strongly suggests that it is a true short-duration GRB.

In Figure 3, we show the rest-frame X-ray luminosity (0.5–4 keV) measured by EP/WXT versus redshifts (left panel) and (0.5–4 keV) X-ray photon index (right). The high luminosity of these sources out to $z\sim5$ is similar to those observed from GRBs, albeit at different energies. In the right panel of Figure 3, we observe a weak trend that the lower-redshift EP events, with intrinsically lower luminosities, have softer X-ray photon indices. This can be explained if their prompt emission spectral peak energies E_p are low, as was the case for EP240414a (Y. Liu et al. 2025) and EP250108a (W. X. Li et al. 2025), which are shown in the left panel of Figure 3 at $z=0.4$ and 0.176, respectively. In this case, the prompt emission emits the bulk of its energy below the gamma-ray band, which can explain the lack of prompt gamma-ray detections. However, we do not only observe EP events without gamma rays to have a steep photon index, and there is a clustering of three events around the synchrotron "line of death" (R. D. Preece et al. 1998).

3.2. Redshift Distribution Comparison

We aim to compare the redshift distribution of EP transients to long-duration GRBs to probe their relationship (Section 2.2). We compare our compiled EP redshifts (Table 1) to the long GRB distribution compiled by the Greiner GRB Catalog.[21] The cumulative distribution function (CDF) of their redshift distributions is shown in the left panel of Figure 4, where we also show the distribution for the two subsamples with and without gamma-ray detections (Figure 4, right panel). To statistically compare these populations, we applied nonparametric two-sample tests on the cumulative redshift distributions. We used both a Kolmogorov–Smirnov (KS) test and Anderson–Darling (AD) test with the null hypothesis that the EP and long GRB redshift distributions are drawn from the same underlying distribution. We have adopted the use of two nonparametric tests specifically because the KS test is most sensitive at the center (near the median) of the distributions, whereas the AD test is efficient at capturing deviations in the tails of the distributions. Therefore, running both tests allows us to probe deviations across the entire distribution.

We performed two-sample KS and AD tests, allowing us to compare two individual samples, i.e., all EP redshifts versus all long GRB redshifts. We made use of the multisample KS test function `ks_2samp` within `SciPy` (P. Virtanen et al. 2020). For the two-sample AD test, the `SciPy` implementation (`anderson_ksamp`) sets a built-in p-value limit of 0.25, and while it does not change our results, we instead opted to use an implementation within the R programming language[22] and wrapped in `Python`.[23] This choice was largely because the p-values for the AD test exceed the cap of $p_{\rm AD}<0.25$ implemented in `SciPy`. We likewise tested a two-sample Cramér–von Mises test (`cramervonmises_2samp` in `SciPy`), which provided similar results that did not change our conclusions. Therefore, for simplicity we focus on the KS and AD test results.

We consider a p-value of $<$0.05 as the boundary below which we reject the null hypothesis, which would suggest that the distributions are different and the samples are unrelated. Instead, we find KS p-values in excess of this threshold ($p_{\rm KS}\gg0.05$), supporting the null hypothesis and implying that the distributions

[21] https://www.mpe.mpg.de/~jcg/grbgen.html
[22] https://search.r-project.org/CRAN/refmans/kSamples/html/ad.test.html
[23] https://rpy2.github.io/doc/latest/html/index.html

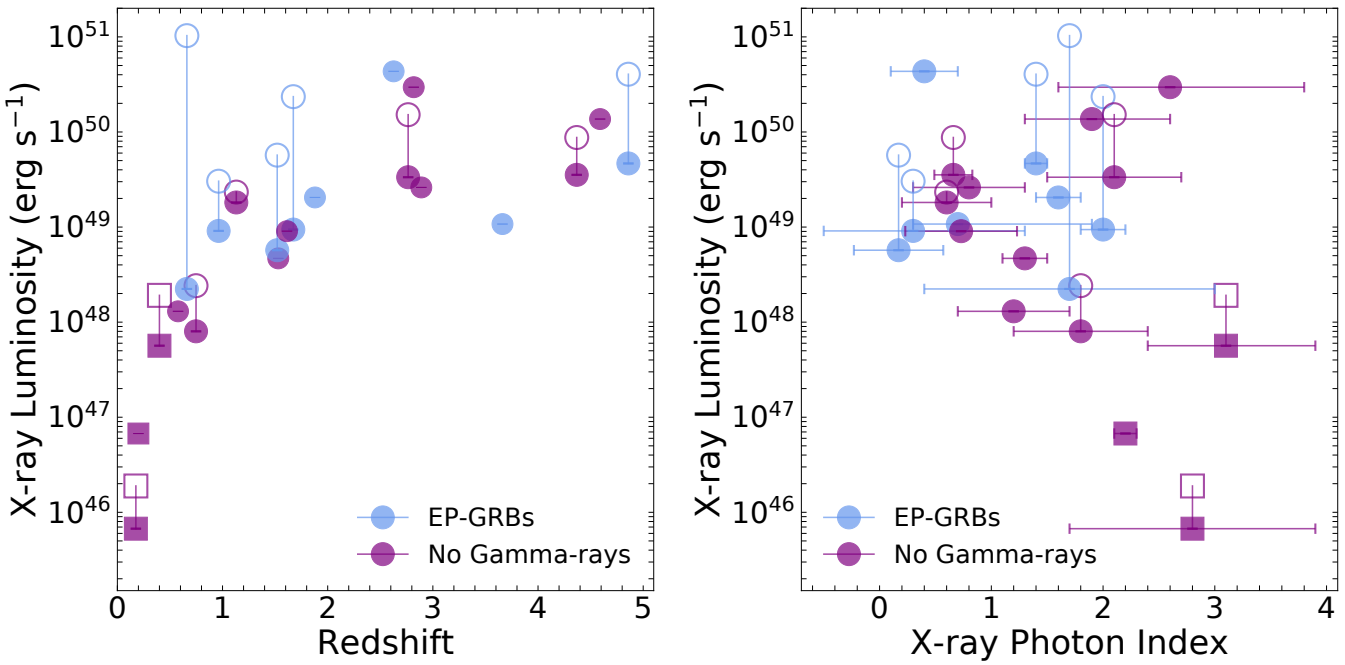

Figure 3. Left: rest-frame 0.5–4 keV X-ray luminosity measured by EP/WXT vs. redshift (Table 1). The time-averaged luminosity is represented by filled symbols, and open symbols refer to the peak luminosity. We have designated between EP-GRBs (blue) and those without gamma rays (purple). Sources represented by squares have been found to be associated with Type Ic-BL supernovae at $z \lesssim 0.4$ (L. Izzo et al. 2025b; J. C. Rastinejad et al. 2025; G. P. Srinivasaragavan et al. 2025a; J. N. D. van Dalen et al. 2025). Right: rest-frame luminosity vs. X-ray photon index measured by EP/WXT. The gray shaded region represents the synchrotron "line of death" (R. D. Preece et al. 1998).

are derived from the same underlying distribution. We find KS p-values of $p_{\rm KS} = 0.43$, 0.34, and 0.45 for the comparison between long-duration GRB redshifts and all EP sources, EP-GRBs, and EP sources without gamma-ray detections, respectively. In all cases, the p-value supports the null hypothesis. The same conclusion is drawn from an AD test, where we find $p_{\rm AD} = 0.47$, 0.24, and 0.33 for all EP sources, EP-GRBs, and EP sources without gamma-ray detections, respectively. These values are compiled in Table 2.

3.2.1. Bootstrap Analysis

In addition, we performed a bootstrap analysis by drawing $N = 10{,}000$ samples and repeating the KS and AD calculation for each sample. We then derived the cumulative distribution of p-values for both statistics. Here we briefly outline the procedure for the sample of all EP redshifts, but note that the same procedure is drawn for the three samples we consider here (all EP, EP-GRBs, and non-GRB EP sources). The procedure is as follows: (i) for a given sample of EP redshifts we produce a bootstrapped data set of the same size (allowing for repetition), (ii) we compute the KS and AD statistic (comparing to the long GRB redshift distribution) using the bootstrapped sample, and (iii) we then repeat this procedure for $N = 10{,}000$ bootstrapped samples. After this, (iv) we compute the 90% confidence interval of the sample of CDFs, which are shown in the left panel of Figure C1 in Appendix C, and (v) we plot the cumulative distribution of p-values, shown in the right panel of Figure C1. We likewise tested allowing for a two-sample bootstrapping approach, where we also produced bootstrapped samples of long GRB redshifts prior to computing the two-sample test statistic. As the long GRB redshift distribution is sufficiently large, this does not have any impact, and our result is the same in either case. This is shown in Figure C1, where it can be seen that they converge to the same cumulative distribution of p-values.

Due to the small sample size of EP events, the distribution of KS p-values from bootstrapping reveals that ∼30% of the bootstrapped sample differs from the long GRB redshift distribution (i.e., $p_{\rm KS} < 0.05$; see Figure C1, Appendix C). For the bootstrapped AD test we find similar fractions of ∼20%–30% with $p_{\rm AD} < 0.05$ (see Figure C2). If the EP redshift distribution is indeed sampled from the long GRB distribution, then increasing the population of EP events with measured redshifts will reveal this more robustly. At present, there is no strong statistical evidence to conclude that they are drawn from separate distributions.

As an example of the strength of this conclusion, we performed the same statistical tests to compare the EP redshifts to those of short-duration GRBs (B. O'Connor et al. 2022). The cumulative distribution of their redshifts is also shown in Figure 4 versus long GRBs and EP redshifts. They are clearly visually distinct. A KS test yields a very convincing rejection of the null hypothesis with $p_{\rm KS} = 1.1 \times 10^{-4}$. We also performed the bootstrap analysis where we allow both the EP redshifts and short GRB redshifts to be resampled with repetition. We note that our result does not change if only one distribution is resampled. Through this bootstrap analysis, we find that 99.2% of samples have a $p_{\rm KS} < 0.05$. This demonstrates that EP transients (at least the majority with redshifts) are unrelated to the compact object mergers that produce short-duration GRBs.

4. Discussion

4.1. The Redshift Distribution of Einstein Probe Transients: Relation to Gamma-Ray Bursts

The redshift distribution of extragalactic transients provides useful information on their progenitors and can be used to constrain their formation pathways. Here we compare the redshift distribution of EP transients to both short and long

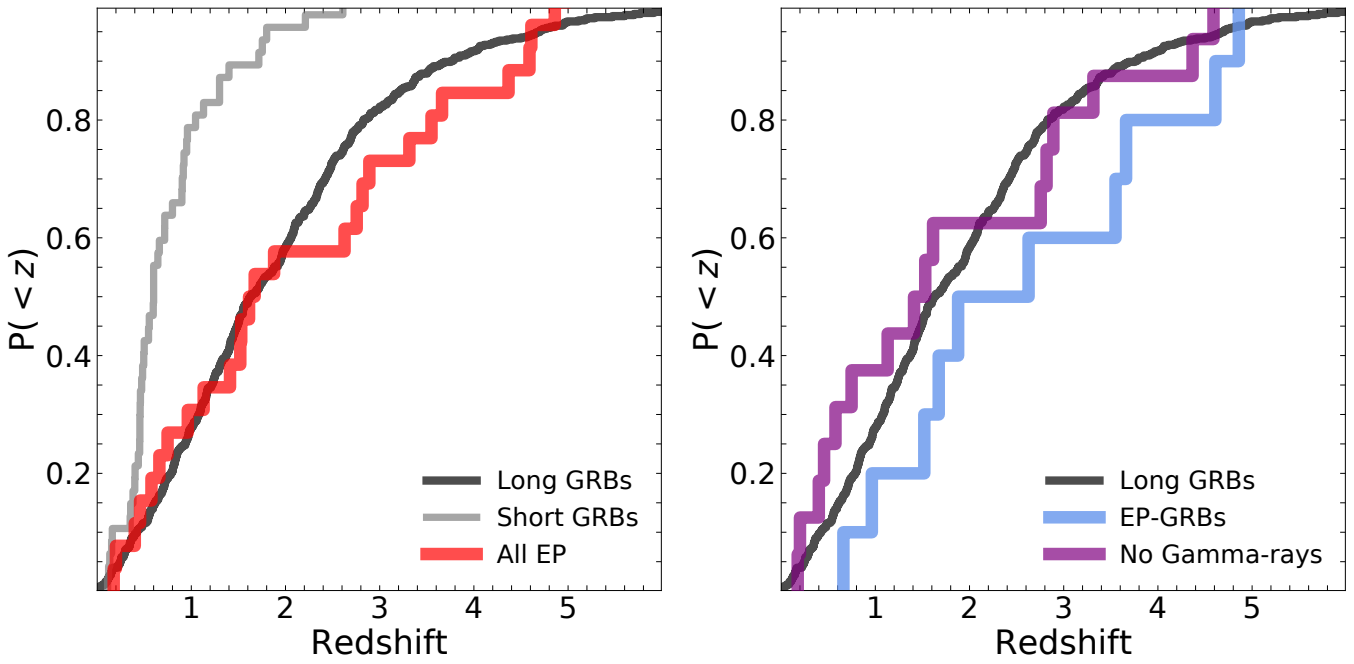

Figure 4. Left: cumulative distribution of the redshift of EP transients (red) compared to short (gray; B. O'Connor et al. 2022) and long (black; Greiner Catalog) GRBs. Right: the EP transients are further divided into those without gamma-ray detections (purple) and those with joint GRB detections (EP-GRBs; blue).

Table 2
A Compilation of the *p*-values Derived in This Work

Sample	$p_{\rm KS}$	$p_{\rm AD}$
All EP	0.43	0.47
EP-GRBs	0.34	0.23
No gamma rays	0.45	0.33

Note. All values refer to KS or AD tests where the sample of EP transient redshifts is compared to the population of long-duration GRB redshifts (Figure 4, left panel).

GRBs (see Figure 4). Due to the broad range of redshifts over which EP transients are discovered (out to $z \sim 5$), we cannot directly compare them to the distributions for optically discovered transients like supernovae. However, GRBs are detected over this redshift range, extending even further back in the Universe's history.

To perform this comparison, we compiled all available redshifts of EP transients from the literature and from GCN Circulars (Table 1; Section 2.2). In total (through 2025 August 29), we identify 26 redshifts for EP transients, 12 of which have joint GRB detections. This comprises ∼23% of publicly reported (extragalactic) EP transients (∼113 in total). The cumulative redshift distribution is shown in Figure 4 for all EP transients (left panel) and the two subpopulations of those with and without GRB associations (right panel).

In Figure 4, we compare these distributions to the short-duration GRB redshift distribution (B. O'Connor et al. 2022) and the long-duration GRB distribution compiled by the Greiner GRB Catalog. The short GRB redshift distribution is obviously inconsistent with a significant deviation, due to the fact that short GRBs are largely undetected[24] at $z > 2$, whereas half of all EP transients lie in that higher redshift range. Instead, the EP redshift distribution very clearly traces the long GRB distribution, signifying that they are likely produced by a similar set of progenitors (massive star collapse), or, at the very least, progenitors that have the same formation rate relative to the star formation history of the Universe (see, e.g., G. Ghirlanda & R. Salvaterra 2022). KS and AD tests (see Section 3.2; Figures C1 and C2) favor that they are drawn from the same underlying distribution with a *p*-value of ∼0.43 (Table 2).

We note that it is known that there is at least some contamination within the population of EP/WXT transients from other classes of events (e.g., stellar flares, X-ray binaries). However, we are confident that at least the extragalactic EP events with measured redshifts and GRB-like (X-ray and optical) afterglows are not coming from these other populations (see Section 2.1), and therefore they do not impact our conclusions. We further compared the distribution of EP transients with and without redshifts in the prompt (0.5–4 keV) X-ray flux and X-ray photon index plane ($F_{\rm X,WXT} - \Gamma_{\rm WXT}$) and verified that the distributions fully overlap with no discernible differences (i.e., both distributions span the same range of photon index and X-ray flux). Therefore, we do not expect selection biases within the extragalactic population of EP transients to play a large role in our conclusions.

While the sample of EP transients is significantly smaller than the hundreds of long GRBs with known redshifts (e.g., J. Hjorth et al. 2012; P. Jakobsson et al. 2012; P. D'Avanzo et al. 2014; D. A. Perley et al. 2016), the current redshift distribution clearly favors a causal connection between EP-detected fast X-ray transients and long-duration GRBs. This is further supported by their overlap in the standard E_p–$E_{\rm iso}$ plane of GRBs (Figure 2). While the current sample of EP transients with reported peak energy E_p constraints is notably small and further analysis will be warranted upon the publication of a full catalog of EP transients, we note that the fact that events like

[24] We note that this is likely a selection effect based on the difficulty to detect and then obtain a redshift for their host galaxies at higher redshifts; see, e.g., B. O'Connor et al. (2022).

EP240315a and EP240801a follow the E_p–$E_{\rm iso}$ strongly supports the hypothesis that EP events should follow these correlations. For example, these two events were missed by standard onboard GRB searches and would not have been detected (or identified) as GRBs without the temporal and spatial localization by EP allowing a targeted subthreshold search. It is therefore strongly implied that many other EP transients could be missed by typical gamma-ray monitors, even in a subthreshold search.

The EP mission is still relatively new (launched in 2024 January), and it will continue to detect high-energy transients in large numbers ($\sim$70 yr^{-1}). As a larger sample of events is built up over the course of the mission, we will eventually be able to separate more clearly into other subclasses of events, such as XRFs, EP-GRBs, and those with "weak" or "failed" jets (e.g., EP250108a; W. X. Li et al. 2025). This will allow for a robust comparison between the redshift, E_p–$E_{\rm iso}$ distributions, and progenitors of these subclasses (see Section 4.2). The specific breakdown of extragalactic EP transients into these subclasses, as well as their relative volumetric rates, is critical information on the deaths of massive stars and their ability to launch collimated relativistic jets (see, e.g., W. X. Li et al. 2025).

4.2. The Separate Subclasses of Extragalactic Einstein Probe Transients: Are They All Collapsars?

Since the 1990s, GRBs have been subdivided based on their hardness ratios and the fraction of energy released at X-ray versus gamma-ray wavelengths. These subdivisions include XRFs and X-ray-rich GRBs (J. Heise et al. 2001; C. Barraud et al. 2003; T. Sakamoto et al. 2005). The narrow soft X-ray band of EP/WXT (without including additional higher-energy instruments) does not allow for the historical hardness ratio definitions (e.g., T. Sakamoto et al. 2004, 2005, 2008) to be applied. However, for a handful of EP-GRBs these definitions can be applied and confirm the transient as an XRF[25] (e.g., EP240801a; S.-Q. Jiang et al. 2025b). The subthreshold gamma-ray detection of many EP-GRBs (Y. H. I. Yin et al. 2024; S.-Q. Jiang et al. 2025b; Y. Liu et al. 2025) suggests that similar events have been missed historically, i.e., that they would not have been uncovered without EP's sensitive soft X-ray capabilities providing the detection necessary to allow a targeted search. This implies a strong selection effect against identifying fast X-ray transients as GRBs or XRFs. This selection effect is likely just misleading observers to conclude they are sources with different properties. Those differences aside, XRFs have generally been considered a natural extension of the GRB phenomena (e.g., J. Heise et al. 2001).

As an added complication, during the era of BATSE, BeppoSAX, and HETE-2 in the late 1990s and early 2000s, there was a more limited number of precise afterglow localizations, resulting in only a handful of redshifts[26] for this class of events (C. Barraud et al. 2003; A. Pélangeon et al. 2008; T. Sakamoto et al. 2008). Despite the limited number of redshifts, the peak energy and fluence correlations were shown to be a natural extension of GRBs (T. Sakamoto et al. 2008), even without calculating their full energy release (Figure 2). This holds for recent EP-GRBs as well; see Figure 2. In this work, we have compared a significant sample of 26 redshifts for EP transients to long GRBs, demonstrating a secure connection between the two classes of events. The close match in their observed redshift distributions supports a shared progenitor population. However, such agreement is not necessarily expected,[27] even under the assumption that both samples originate from the same progenitor, due to the likelihood of differing selection effects between EP/WXT and traditional high-energy monitors.[28] These possible selection biases may account for slight discrepancies between the distributions that could become more evident with a larger EP sample.

For instance, it has been proposed that EP events should preferentially detect GRBs that are off-axis (H.-X. Gao et al. 2025), mildly relativistic (e.g., M. Busmann et al. 2025), or at higher redshift (J.-J. Wei & X.-F. Wu 2025), all of which are predicted to have lower peak energies in the observer frame. However, at present there is no strong evidence that EP preferentially detects higher-redshift events at a higher rate than standard gamma-ray monitors. While this could explain subtle shifts in the redshift distribution, such as the mild excess of high-redshift events at $z > 2$ (Figure 4), the current evidence is insufficient to conclude that EP detects higher-redshift events at an elevated rate. This observed deviation may be a statistical fluctuation given the modest sample size and could even out with time. Moreover, it is unlikely that redshift is the dominant factor in determining the observed peak energy, as significant scatter is an intrinsic property of GRBs (Figure 2).

Despite this close connection to long GRBs, EP has uncovered a variety of peculiar transients that are missed by traditional gamma-energy monitors (Figure 3). These include candidate relativistic jetted tidal disruption events (EP240408a, B. O'Connor et al. 2025c; W. Zhang et al. 2025; EP250702a/GRB 250702B, J. Carney et al. 2025; B. P. Gompertz et al. 2025; A. J. Levan et al. 2025b; E. Neights et al. 2025; B. O'Connor et al. 2025a) and multiple events with extreme optical rebrightening episodes (EP240414a and EP241021a; M. Busmann et al. 2025; J. N. D. van Dalen et al. 2025). The physical origin of these rapid ($\sim$1 day) and large-amplitude ($\sim$ 1 mag) rebrightening episodes are debated. While it has been proposed that discrete refreshed shocks provide the most straightforward explanation (M. Busmann et al. 2025; S. Srivastav et al. 2025), alternative models suggest that the initially fading emission is due to a cocoon produced by the interaction of the jet with an extended stellar envelope (G. Gianfagna et al. 2025; H. Hamidani et al. 2025; J. N. D. van Dalen et al. 2025; J.-H. Zheng et al. 2025). In the latter case, the jet could either be mildly relativistic or an ultrarelativistic outflow viewed off-axis (M. Yadav et al. 2025; J.-H. Zheng et al. 2025).

EP has also revealed rare transient classes with unprecedented frequency. For example, it has already detected two relativistic shock breakout candidates (EP250108a and

[25] It should be noted that standard XRF definitions rely on the observed peak energy (e.g., <20 keV; A. Pélangeon et al. 2008), which is not the same as an intrinsic XRF, where the intrinsic (redshift-corrected) peak energy is <20 keV (e.g., T. Sakamoto et al. 2004). We note that the majority of HETE-2 events with measured redshifts are not intrinsic XRFs (Figure 2).

[26] A literature search revealed only $\sim$20 redshifts for HETE-2 events overall, with only six (observed) XRFs having a measured redshift (T. Sakamoto et al. 2005; A. Pélangeon et al. 2008).

[27] We note that there is a difference between an observed vs. intrinsic redshift distribution, where the observed distribution depends heavily on the minimum observable fluence and whether a sample is volume limited.

[28] For example, see Figure 14 of A. Pélangeon et al. (2008), which shows that the HETE-2 redshift distribution deviates from the early Swift redshift sample.

EP250304a; R. A. J. Eyles-Ferris et al. 2025; L. Izzo et al. 2025b; J. C. Rastinejad et al. 2025; G. P. Srinivasaragavan et al. 2025a), already exceeding the (observed) rate in the past 20 yr from Swift (S. Campana et al. 2006; A. M. Soderberg et al. 2006). These are among the few EP events (all lacking gamma rays and at $z < 0.4$; Figure 3) associated with Type Ic-BL supernovae, the same supernovae generally associated with long-duration GRBs and their collapsar progenitors (S. E. Woosley & J. S. Bloom 2006; J. Hjorth & J. S. Bloom 2012). That these low-redshift EP transients show clear supernova signatures is consistent with our interpretation that many EP transients originate from the deaths of massive stars. In the case of EP250108a, it has also been suggested that the jet potentially failed to break out of its stellar envelope owing to an extended circumstellar envelope (R. A. J. Eyles-Ferris et al. 2025; G. P. Srinivasaragavan et al. 2025a). Therefore, while EP is very likely identifying events that are driven by the same progenitors as long GRBs (tracing the same redshift distribution that closely follows star formation), these events also cover a parameter space that is not probed by standard gamma-ray-only triggers and are likely the predicted missing population of failed jets and dirty fireballs (J. E. Rhoads 2003) with lower bulk Lorentz factors.

Nevertheless, the EP sample is unlikely to be composed solely of collapsars. While we have filtered out Galactic contaminants, extragalactic events such as EP250704a fall within the region typically occupied by short GRBs in the E_p–$E_{\rm iso}$ plane (see Figure 2; D. Frederiks et al. 2025b) and may be associated with compact object mergers. Importantly, the inclusion or exclusion of such events has negligible impact on our statistical conclusions. For example, removing EP250704a from our sample results in only a marginal change in p-values (remaining at $\approx$0.3) from both KS and AD tests and does not modify our conclusion (see Section 3.2). As the sample grows, the identification and influence of potential contaminants (e.g., short GRBs) will become clearer and less significant to the overall population.

The volumetric rates of EP transients remain poorly constrained, but preliminary estimates suggest that they may be comparable to or exceed those of standard GRBs. For EP240414a, H. Sun et al. (2025) set a lower limit of $0.3\,{\rm Gpc^{-3}\,yr^{-1}}$ to its volumetric rate. For EP250108a, W. X. Li et al. (2025) derived $7.3^{+16.8}_{-6.0}\,{\rm Gpc^{-3}\,yr^{-1}}$. After correcting for the redshift completeness of EP transients, they find a corrected rate of $29.2^{+67.2}_{-24.0}\,{\rm Gpc^{-3}\,yr^{-1}}$ (W. X. Li et al. 2025). This is comparable to the volumetric rate of low-luminosity GRBs ($\sim 100\,{\rm Gpc^{-3}\,yr^{-1}}$) like GRB 060218 (A. M. Soderberg et al. 2006) and significantly exceeds that of typical high-luminosity GRBs ($1.3^{+0.6}_{-0.7}\,{\rm Gpc^{-3}\,yr^{-1}}$; D. Wanderman & T. Piran 2010)—where for both low- and high-luminosity GRBs the rates above correspond to events that are beamed toward Earth. This supports a scenario in which weak or failed jets are intrinsically more common than successful ones, as well as that prior selection biases against soft X-ray transients hindered their discovery. As EP continues to expand the sample of such events, our understanding of their origins, diversity, and true rates will improve significantly.

5. Conclusions

In this work, we compared the cumulative redshift distributions of EP fast X-ray transients and long-duration GRBs using nonparametric two-sample tests. These tests reveal that the distributions are statistically indistinguishable, supporting that their redshift distributions are drawn from the same underlying population. Therefore, the fraction of EP transients related to GRBs is higher than would be expected based on gamma-ray associations alone. We conclude that a substantial fraction of EP transients, at the very least those with measured redshifts, originate from similar massive star progenitors (collapsars) as long-duration GRBs. This is supported by the similar redshift distribution for EP transients both with and without prompt gamma-ray detections, as well as their continuity with long GRBs in the E_p–$E_{\rm iso}$ plane.

Several mechanisms can suppress a gamma-ray detection from otherwise GRB-like explosions (e.g., weak or trapped jets, slightly off-axis viewing angles, lower bulk Lorentz factors, or limited instrument sensitivity). The low-z ($z < 0.4$) subsample, in particular, is consistent with prompt spectra peaking in the soft X-ray band, naturally explaining the absence of high-energy triggers. While small number statistics and selection effects remain, our redshift and prompt emission comparisons support a predominantly massive star origin for EP fast X-ray transients. Our results reinforce similar conclusions drawn between XRFs and GRBs based on BATSE, BeppoSAX, and HETE-2.

Acknowledgments

The authors acknowledge the referee for their careful review of the manuscript. The authors thank the Einstein Probe team for their public release of onboard WXT triggers that enables multiwavelength follow-up. B.O. acknowledges useful discussions with Dheeraj Pasham, Igor Andreoni, Jamie Kennea, and Jimmy DeLaunay. M.B. acknowledges Fabian Schüssler for assistance with the Astro-COLIBRI platform. B.O. thanks Rosa Becerra and Massine El Kabir for their aid in obtaining X-shooter spectra.

B.O. is supported by the McWilliams Postdoctoral Fellowship in the McWilliams Center for Cosmology and Astrophysics at Carnegie Mellon University. M.B. is supported by a Student Grant from the Wübben Stiftung Wissenschaft. This work benefited from travel support for M.B. from the McWilliams Visitors Program as part of the McWilliams Center for Cosmology and Astrophysics at Carnegie Mellon University. P.B. is supported by a grant (No. 2020747) from the United States–Israel Binational Science Foundation (BSF), Jerusalem, Israel, by a grant (No. 1649/23) from the Israel Science Foundation, and by a grant (No. 80NSSC 24K0770) from the NASA astrophysics theory program. E.T., N.P., and Y.Y. are supported by the European Research Council through the Consolidator grant BHianca (grant agreement ID 101002761).

Based on observations obtained at the international Gemini Observatory, a program of NSF's OIR Lab, which is managed by the Association of Universities for Research in Astronomy (AURA) under a cooperative agreement with the National Science Foundation on behalf of the Gemini Observatory partnership: the National Science Foundation (United States), National Research Council (Canada), Agencia Nacional de Investigación y Desarrollo (Chile), Ministerio de Ciencia, Tecnología e Innovación (Argentina), Ministério da Ciência, Tecnologia, Inovações e Comunicações (Brazil), and Korea Astronomy and Space Science Institute (Republic of Korea). The data were acquired through the Gemini Observatory Archive at NSF NOIRLab and processed using Data Reduction

for Astronomy from Gemini Observatory North and South (DRAGONS). Based on observations collected at the European Organisation for Astronomical Research in the Southern Hemisphere under ESO program(s) 114.27LW.

Facilities: EP, Gemini:South, VLT:Kueyen.

Software: `Astropy` (Astropy Collaboration et al. 2018, 2022), `SciPy` (P. Virtanen et al. 2020), `DRAGONS` (K. Labrie et al. 2019; K. Labrie et al. 2023), X-shooter pipeline (P. Goldoni 2011), `zHunter` (J. T. Palmerio 2025).

Appendix A
Optical Spectroscopy with Gemini and the VLT

Here we report on three spectroscopic redshifts of EP transients obtained through our programs on the Gemini South Telescope and the Very Large Telescope (VLT). The spectra are shown in Figure A1.

A.1. EP250302a

We carried out ultraviolet to near-infrared spectroscopy of EP250302a with the VLT located at Cerro Paranal, Chile, using the X-shooter spectroscopy (J. Vernet et al. 2011) under program 114.27LW (PI: Troja). Observations with the X-shooter spectrograph mounted on the ESO VLT UT3 (Melipal) began on 2025 March 3 at 05:14:45 UT, corresponding to $T_0 + 13.6$ hr, for 4×600 s. The data were reduced using the standard X-shooter pipeline (P. Goldoni 2011) and revealed a trace in all three arms (UVB, VIS, NIR). In the UVB arm, we identify multiple narrow absorption features associated with Fe II$_{\lambda 2600,2587,2383,2374,2344}$ at redshift $z = 1.1310 \pm 0.0002$. A zoom-in on the spectrum showing these features is displayed in Figure A1. This determination is consistent with earlier reports for the redshift (L. Izzo et al. 2025a; Y.-H. Yang et al. 2025b). We further identify an

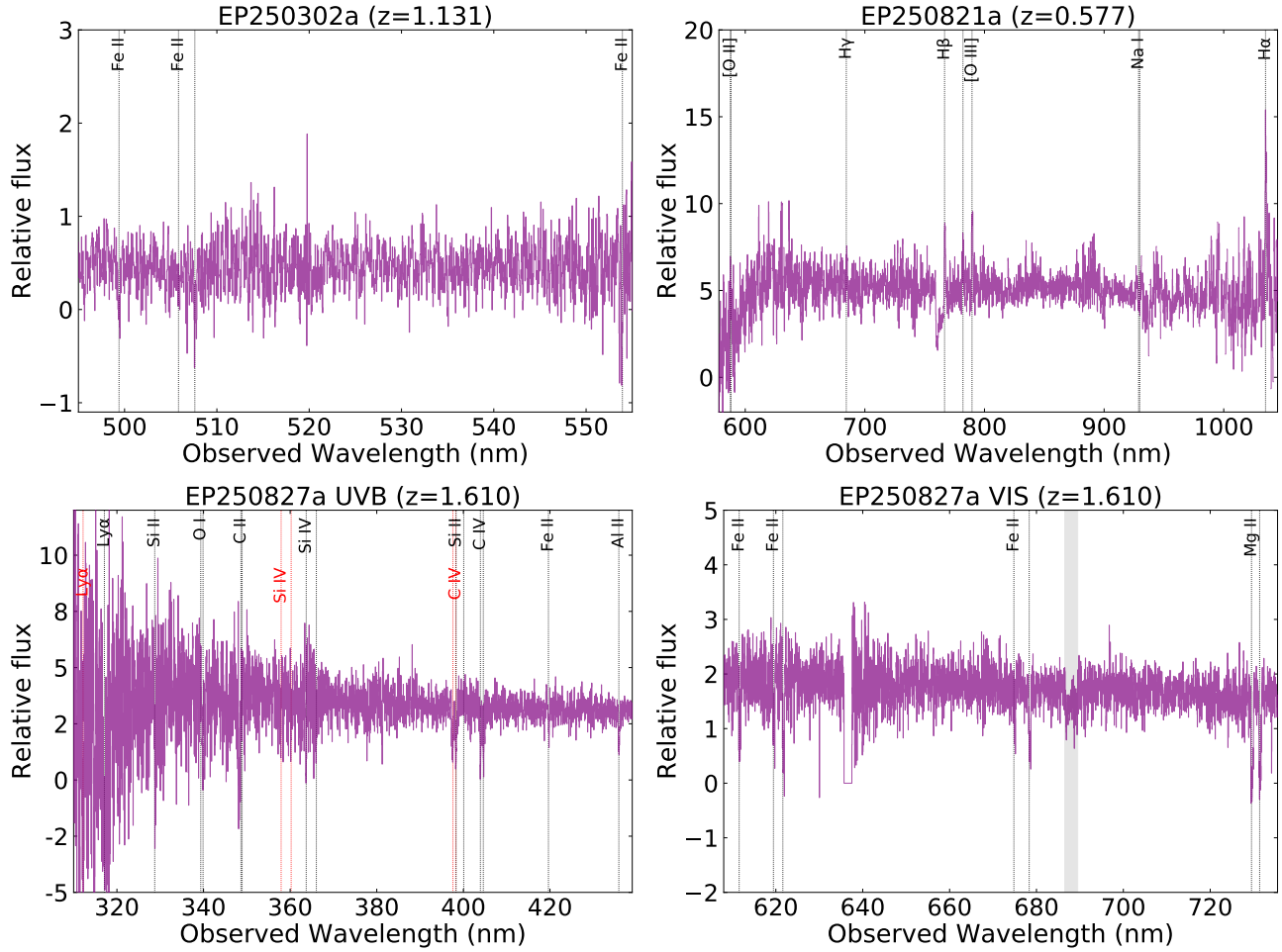

Figure A1. Spectroscopy of EP250302a (VLT X-shooter), EP250821a (Gemini South GMOS), and EP250827a (VLT X-shooter) used to measure their redshifts. For EP250827a, due to the large number of absorption lines, we show both the UVB and VIS arms of the X-shooter spectrum. The spectra have not been smoothed or rebinned.

intervening absorber at $z = 0.549$, as reported by Y.-H. Yang et al. (2025a). No other absorbers or unidentified absorption lines are discovered, so we consider the redshift secure. As we do not identify any fine-structure absorption lines at $z = 1.1310$, we cannot exclude a higher redshift. However, we detect a weak trace down to 370 nm, which sets an upper limit of $z < 2.0$ to the redshift of EP250302a.

A.2. EP250821a

We observed EP250821a with the Gemini GMOS-S spectrograph starting on 2025 August 26 at 01:53:43 UT under program GS-2025A-FT-111 (PI: O'Connor). Our spectra cover wavelengths 575–1060 nm and consist of 4×1200 s exposures using the R400 grating. The data were reduced using the DRAGONS software (K. Labrie et al. 2019; K. Labrie et al. 2023). We detect multiple emission lines from the underlying host galaxy, including the [O II]$_{\lambda3727,3729}$ doublet, [O III]$_{\lambda4960,5007}$, Hβ, and Hα, at a consistent redshift of $z = 0.5775 \pm 0.0003$ as initially reported by J. An et al. (2025a) and B. O'Connor et al. (2025b). We also detect [Na I] absorption and the 4000 Å break at this redshift. We note that J. An et al. (2025a) reported the identification of multiple narrow absorption features in an earlier optical spectrum obtained ∼4 days prior. This supports our redshift determination from host galaxy emission lines (Figure A1).

A.3. EP250827a

We observed GRB 250827A with the VLT X-shooter spectrograph under program 114.27LW (PI: Troja) starting on 2025 August 27 at 09:21:51 UT, corresponding to $T_0 + 1.67$ hr, for 4×600 s. The data were reduced using the standard X-shooter pipeline (P. Goldoni 2011). Our spectrum reveals a large number of significant absorption features. We identify >20 narrow absorption lines between the UVB and VIS arms consisting of Si II$_{\lambda1260,1304}$, O I$_{\lambda1302}$, C II$_{\lambda1334,1335}$, Si IV$_{\lambda1394,1403,1527,1533}$, C IV$_{\lambda1548,1550}$, Fe II$_{\lambda1608}$, Al II$_{\lambda1671}$, and Al III$_{\lambda1855,1863}$ in the UVB arm and Fe II$_{\lambda2344,2345,2382,2383,2384,2587,2600}$ and Mg II$_{\lambda2796,2804}$ in the VIS arm. These features are all at a common redshift of $z = 1.6105 \pm 0.0003$. The existence of fine-structure lines secures the redshift of the GRB. We zoom in on a few of these features in Figure A1. This redshift is consistent with previous reports by A. J. Levan et al. (2025e) and N. Passaleva et al. (2025). We identify a marginal broad absorption feature at the blue end of the UVB arm that could be associated with Lyα at this redshift of $z = 1.6105$. This is supported by the detection of a blue trace down to 320 nm, which sets an upper limit to the redshift of $z < 1.63$. This is consistent with the lack of detection of any additional higher-redshift absorption features. We do, however, identify an intervening absorber at $z = 1.5688$ owing to measuring narrow Si IV$_{\lambda1394,1403}$ and C IV$_{\lambda1548,1550}$ absorption lines. No other absorbers or unidentified absorption lines are discovered. As such, we consider the redshift secure.

Appendix B
Comments on Redshifts Based on Host Galaxy Emission Lines

The transients with redshifts based on emission lines from their underlying host galaxies are EP240414a (S. Srivastav et al. 2025; J. N. D. van Dalen et al. 2025), EP241107A (J. A. Quirola-Vásquez et al. 2025), EP241113a (J. A. Quirola-Vásquez et al. 2024b), EP241217b/GRB 241217A (B. Schneider et al. 2024), EP250416a/ GRB 250416C (A. J. Levan et al. 2025c), and EP250821a (Section A.2; J. An et al. 2025a; B. O'Connor et al. 2025b). We note that in the case of EP250821a (Figure A1) J. An et al. (2025a) also reported absorption features. In particular, the redshifts for EP241113a, EP241217b, and EP250416a are tentative, as they are based on a single emission line that is interpreted as [O III]$_{\lambda5007}$ for EP241217b (B. Schneider et al. 2024) and the [O II]$_{\lambda3727,3729}$ doublet for EP241113a (J. A. Quirola-Vásquez et al. 2024b) and EP250416a (A. J. Levan et al. 2025c). We note that the redshift of EP240414a is more secure, as the galaxy's redshift matches the distance inferred from supernova features in a sequence of optical spectra (J. N. D. van Dalen et al. 2025). We have excluded EP250207B from our sample, due to its uncertain redshift (P. G. Jonker et al. 2025, R. L. Becerra et al. 2025, in preparation), but note that the exclusion of this single event does not impact our conclusions.

Appendix C
Bootstrap Analysis Results

We performed a bootstrap analysis between the EP redshift distribution and the redshift distribution of long GRBs (see Section 3.2). The cumulative distributions of bootstrapped p-values computed using the KS test are displayed in Figure C1, and the distributions for the AD test are shown in Figure C2. We find that ∼30% of bootstrapped samples yield a KS test p-value $p_{\rm KS} < 0.05$ and ∼20%–30% for the AD test with $p_{\rm AD} < 0.05$.

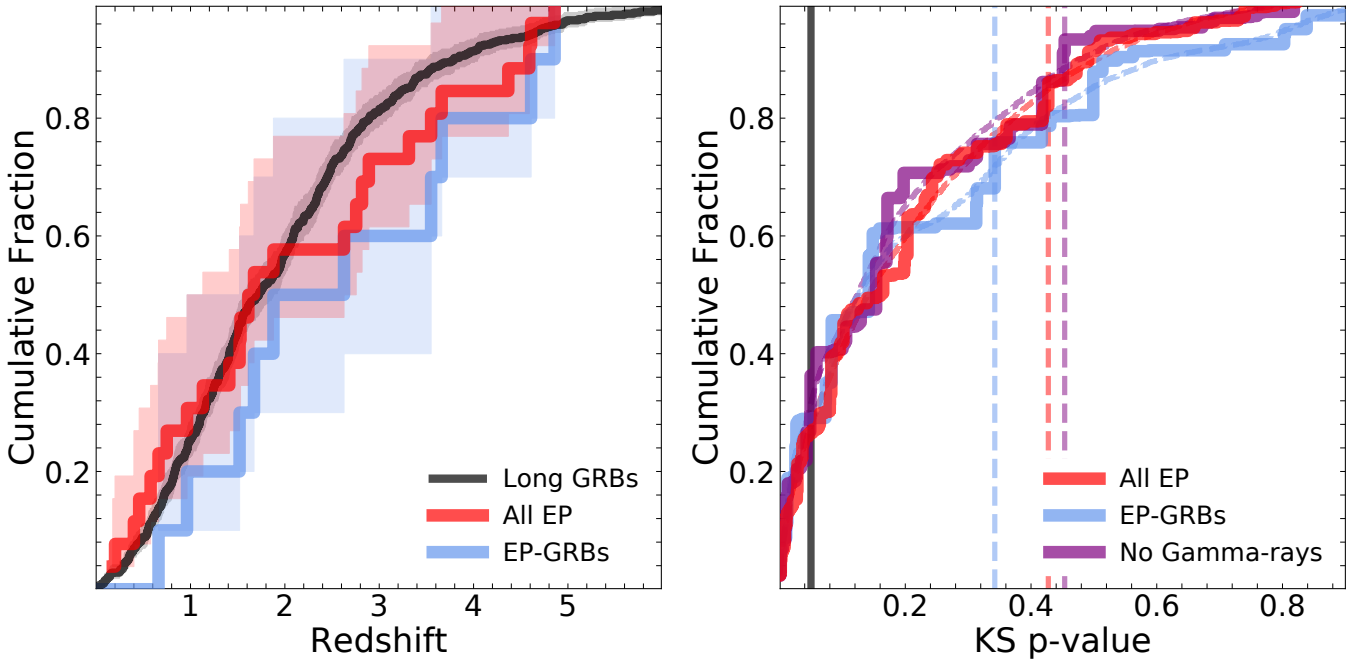

Figure C1. Left: cumulative distribution of the redshift of EP transients (red) compared to EP-GRBs (blue) and long GRBs (black). The shaded regions show the 90% confidence regions of the CDFs after bootstrapping $N = 10{,}000$ times. To avoid further crowding the figure, we do not display the EP subsample without gamma rays. Right: cumulative distribution of KS p-values obtained from bootstrapping. We show the p-value distributions for all EP transients (red), EP-GRBs (blue), and those without prompt gamma-ray detections (purple). The thin-line CDFs are computed when also bootstrapping the long GRB distribution, whereas the thick solid lines are determined when only bootstrapping the three EP distributions. The vertical lines show the p-value for the measured sample without any bootstrapping. The solid black line denotes $p = 0.05$, below which the null hypothesis is rejected.

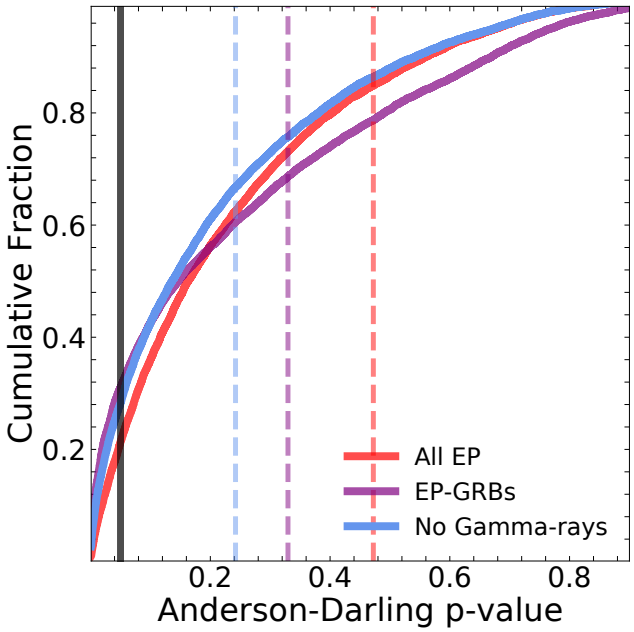

Figure C2. Cumulative distribution of AD p-values obtained from bootstrapping. We show the p-value distributions for all EP transients (red), EP-GRBs (blue), and those without prompt gamma-ray detections (purple). The vertical lines show the p-value for the measured sample without any bootstrapping. The solid black line denotes $p = 0.05$, below which the null hypothesis is rejected.

ORCID iDs

Brendan O'Connor https://orcid.org/0000-0002-9700-0036
Paz Beniamini https://orcid.org/0000-0001-7833-1043
Eleonora Troja https://orcid.org/0000-0002-1869-7817
Malte Busmann https://orcid.org/0009-0001-0574-2332
Simone Dichiara https://orcid.org/0000-0001-6849-1270
Ramandeep Gill https://orcid.org/0000-0003-0516-2968
Jonathan Granot https://orcid.org/0000-0001-8530-8941
Michael J. Moss https://orcid.org/0000-0002-1103-7082
Xander J. Hall https://orcid.org/0000-0002-9364-5419
Antonella Palmese https://orcid.org/0000-0002-6011-0530
Niccolò Passaleva https://orcid.org/0009-0007-6886-4082
Yu-Han Yang https://orcid.org/0000-0003-0691-6688

References

Amati, L. 2006, MNRAS, 372, 233
Amati, L., D'Agostino, R., Luongo, O., Muccino, M., & Tantalo, M. 2019, MNRAS, 486, L46
Amati, L., Frontera, F., & Guidorzi, C. 2009, A&A, 508, 173
Amati, L., Frontera, F., Tavani, M., et al. 2002, A&A, 390, 81
Amati, L., Guidorzi, C., Frontera, F., et al. 2008, MNRAS, 391, 577
An, J., Abril-Melgarejo, V., Eyles-Ferris, R. A. J., et al. 2025a, GCN, 41490, 1
An, J., Malesani, D. B., Xu, D., et al. 2025b, GCN, 40966, 1
Aryan, A., Chen, T.-W., Yang, S., et al. 2025, arXiv:2504.21096
Astropy Collaboration, Price-Whelan, A. M., Lim, P. L., et al. 2022, ApJ, 935, 167
Astropy Collaboration, Price-Whelan, A. M., Sipőcz, B. M., et al. 2018, AJ, 156, 123
Barraud, C., Olive, J. F., Lestrade, J. P., et al. 2003, A&A, 400, 1021
Barthelmy, S. D., Barbier, L. M., Cummings, J. R., et al. 2005, SSRv, 120, 143
Bloom, J. S., Kulkarni, S. R., & Djorgovski, S. G. 2002, AJ, 123, 1111
Bochenek, A., Xu, D., Zhu, Z. P., et al. 2024, GCN, 37039, 1
Burrows, D. N., Hill, J. E., Nousek, J. A., et al. 2005, SSRv, 120, 165
Busmann, M., O'Connor, B., Sommer, J., et al. 2025, A&A, 701, A225
Campana, S., Mangano, V., Blustin, A. J., et al. 2006, Natur, 442, 1008
Carney, J., Andreoni, I., O'Connor, B., et al. 2025, arXiv:2509.22784
Chen, Y., Wang, J., Yang, Y., et al. 2025, RDTM, 9, 198
Cheng, H. Q., Zhao, G. Y., Zhou, C., et al. 2025, GCN, 40906, 1
Chornock, R., Hammerstein, E., & Guo, X. 2025, GCN, 40265, 1
Dai, C. Y., Zhao, Y. Q., Mao, X., et al. 2025, GCN, 39556, 1
D'Avanzo, P., Salvaterra, R., Bernardini, M. G., et al. 2014, MNRAS, 442, 2342

de Ugarte Postigo, A., Malesani, D. B., Martin-Carrillo, A., et al. 2025, GCN, 39160, 1
Dichiara, S., Troja, E., Beniamini, P., et al. 2021, ApJL, 911, L28
Eyles-Ferris, R. A. J., Jonker, P. G., Levan, A. J., et al. 2025, ApJL, 988, L14
Fermi GBM Team 2025a, GCN, 39327, 1
Fermi GBM Team 2025b, GCN, 39479, 1
Frail, D. A., Kulkarni, S. R., Nicastro, L., Feroci, M., & Taylor, G. B. 1997, Natur, 389, 261
Frederiks, D., Lysenko, A., Ridnaia, A., et al. 2024, GCN, 37071, 1
Frederiks, D., Lysenko, A., Ridnaia, A., et al. 2025a, GCN, 40087, 1
Frederiks, D., Lysenko, A., Ridnaia, A., et al. 2025b, GCN, 40972, 1
Gao, H.-X., Geng, J.-J., Liang, Y.-F., et al. 2025, ApJ, 986, 106
Gehrels, N., Chincarini, G., Giommi, P., et al. 2004, ApJ, 611, 1005
Ghirlanda, G., & Salvaterra, R. 2022, ApJ, 932, 10
Gianfagna, G., Piro, L., Bruni, G., et al. 2025, arXiv:2505.05444
Goldoni, P. 2011, AN, 332, 227
Gompertz, B. P., Levan, A. J., Laskar, T., et al. 2025, arXiv:2509.22778
Granot, J., & Sari, R. 2002, ApJ, 568, 820
Hamidani, H., Sato, Y., Kashiyama, K., et al. 2025, ApJL, 986, L4
Heise, J., Zand, J. I., Kippen, R. M., & Woods, P. M. 2001, in Gamma-ray Bursts in the Afterglow Era, ed. E. Costa, F. Frontera, & J. Hjorth (Berlin: Springer-Verlag), 16
Hjorth, J., & Bloom, J. S. 2012, in Chapter 9 in "Gamma-Ray Bursts, ed. C. Kouveliotou, R. A. M. J. Wijers, & S. Woosley (Cambridge: Cambridge Univ. Press), 169
Hjorth, J., Malesani, D., Jakobsson, P., et al. 2012, ApJ, 756, 187
Hu, D. F., Cheng, H. Q., Yang, Z. H., et al. 2025, GCN, 39833, 1
Izzo, L., Eyles-Ferris, R. A. J., Xu, D., et al. 2025a, GCN, 39564, 1
Izzo, L., Martin-Carrillo, A., Malesani, D. B., et al. 2025b, GCN, 39851, 1
Jakobsson, P., Hjorth, J., Malesani, D., et al. 2012, ApJ, 752, 62
Jiang, S.-Q., Wang, B. T., Wu, H. Z., et al. 2025a, GCN, 39513, 1
Jiang, S.-Q., Xu, D., van Hoof, A. P. C., et al. 2025b, arXiv:2503.04306
Jonker, P. G., Levan, A. J., Liu, X., et al. 2025, arXiv:2508.13039
Klingler, N. J., Dichiara, S., Gupta, R., et al. 2024, GCN, 37956, 1
Kouveliotou, C., Meegan, C. A., Fishman, G. J., et al. 1993, ApJL, 413, L101
Labrie, K., Anderson, K., Cárdenes, R., Simpson, C., & Turner, J. E. H. 2019, in ASP Conf. Ser. 523, Astronomical Data Analysis Software and Systems XXVII, ed. P. J. Teuben et al. (San Francisco, CA: ASP), 321
Labrie, K., Simpson, C., Cardenes, R., et al. 2023, RNAAS, 7, 214
Levan, A. J., Izzo, L., Malesani, D. B., et al. 2025a, GCN, 39438, 1
Levan, A. J., Jonker, P. G., Saccardi, A., et al. 2024a, arXiv:2404.16350
Levan, A. J., Martin-Carrillo, A., Laskar, T., et al. 2025b, ApJL, 990, L28
Levan, A. J., Quirola-Vásquez, J., Jonker, P. G., et al. 2025c, GCN, 40219, 1
Levan, A. J., Quirola-Vásquez, J. A., Bauer, F. E., et al. 2025d, GCN, 39027, 1
Levan, A. J., Quirola-Vásquez, J. A., Jonker, P. G., et al. 2025e, GCN, 41557, 1
Levan, A. J., Quirola-Vásquez, J. A., Rastinejad, J. C., et al. 2024b, GCN, 38593, 1
Li, A., Cheng, Y. H., Zhou, C., et al. 2025, GCN, 40956, 1
Li, R. Z., Chen, W., Chatterjee, K., et al. 2024, GCN, 38171, 1
Li, R. Z., Wang, B. T., Song, F. F., et al. 2025, GCN, 40084, 1
Li, W. X., Zhu, Z. P., Zou, X. Z., et al. 2025, arXiv:2504.17034
Liang, Y. F., Hu, D. F., Jin, C. C. & Einstein Probe Team 2025, GCN, 41467, 1
Liu, Y., Sun, H., Xu, D., et al. 2025, NatAs,
Liu, Z. Y., Huang, M. Q., Dai, C. Y., et al. 2024, GCN, 38211, 1
Liu, Z. Y., Zhang, M. H., Liu, M. J., et al. 2025, GCN, 39165, 1
MacFadyen, A. I., & Woosley, S. E. 1999, ApJ, 524, 262
Marius, B., Francis, F., Damien, T., et al. 2024, GCN, 38594, 1
Meegan, C., Lichti, G., Bhat, P. N., et al. 2009, ApJ, 702, 791
Neights, E., Burns, E., Fryer, C. L., et al. 2025, arXiv:2509.22792
Ni, K. R., Hua, Y. L., Liu, M. J., et al. 2025, GCN, 41573, 1
O'Connor, B., Gill, R., DeLaunay, J., et al. 2025a, arXiv:2509.22787
O'Connor, B., Hall, X., & Palmese, A. 2025b, GCN, 41549, 1
O'Connor, B., Pasham, D., Andreoni, I., et al. 2025c, ApJL, 979, L30
O'Connor, B., Troja, E., Dichiara, S., et al. 2022, MNRAS, 515, 4890
Palmerio, J. T. 2025, zHunter, v0.10., GitHub, https://github.com/JPalmerio/zHunter
Passaleva, N., Becerra, R. L., El Kabir, M., Yang, Y.-Y., & Troja, E. 2025, GCN, 41570, 1
Pélangeon, A., Atteia, J. L., Nakagawa, Y. E., et al. 2008, A&A, 491, 157
Pérez-Fournon, I., Sun, N. C., Li, W., et al. 2024, GCN, 37858, 1
Perley, D. A., Krühler, T., Schulze, S., et al. 2016, ApJ, 817, 7
Planck Collaboration, Aghanim, N., Akrami, Y., et al. 2020, A&A, 641, A6
Poolakkil, S., Preece, R., Fletcher, C., et al. 2021, ApJ, 913, 60
Preece, R. D., Briggs, M. S., Mallozzi, R. S., et al. 1998, ApJL, 506, L23
Pugliese, G., Xu, D., Izzo, L., et al. 2024, GCN, 37852, 1
Quirola-Vásquez, J. A., Bauer, F. E., Jonker, P. G., et al. 2022, A&A, 663, A168
Quirola-Vásquez, J. A., Bauer, F. E., Jonker, P. G., et al. 2023, A&A, 675, A44
Quirola-Vásquez, J. A., Bauer, F. E., Jonker, P. G., Malesani, D. B., & Levan, A. J. 2025, GCN, 38126, 1
Quirola-Vásquez, J. A., Jonker, P. G., Levan, A. J., et al. 2024a, GCN, 37087, 1
Quirola-Vásquez, J. A., Jonker, P. G., Stern, D., et al. 2024b, GCN, 38449, 1
Quirola-Vásquez, J. A., van Dalen, J., Malesani, D. B., et al. 2024c, GCN, 37013, 1
Rastinejad, J. C., Levan, A. J., Jonker, P. G., et al. 2025, ApJL, 988, L13
Ravasio, M. E., Burns, E., Goldstein, A., Jonker, P. G. & Fermi-GBM Team 2025, GCN, 40262, 1
Ravasio, M. E., Veres, P., Hamburg, R., et al. 2024, GCN, 38625, 1
Reichherzer, P., Schüssler, F., Lefranc, V., et al. 2021, ApJS, 256, 5
Rhoads, J. E. 2003, ApJ, 591, 1097
Ricci, R., Troja, E., Yang, Y.-H., et al. 2025, ApJL, 979, L28
Roming, P. W. A., Kennedy, T. E., Mason, K. O., et al. 2005, SSRv, 120, 95
Saccardi, A., Abril-Melgarejo, V., Zhu, Z. P., et al. 2025a, GCN, 40266, 1
Saccardi, A., Levan, A. J., Zhu, Z., et al. 2024, GCN, 35936, 1
Saccardi, A., Sadibekova, T., Dagoneau, N., et al. 2025b, GCN, 39154, 1
Saccardi, A., Zhu, Z. P., Schneider, B., et al. 2025c, GCN, 39585, 1
Sakamoto, T., Hullinger, D., Sato, G., et al. 2008, ApJ, 679, 570
Sakamoto, T., Lamb, D. Q., Graziani, C., et al. 2004, ApJ, 602, 875
Sakamoto, T., Lamb, D. Q., Kawai, N., et al. 2005, ApJ, 629, 311
Sanchez-Ramirez, R., Castro-Tirado, A. J., Caballero-Garcia, M. D., et al. 2025, GCN, 39343, 1
Sari, R., Piran, T., & Narayan, R. 1998, ApJL, 497, L17
Schneider, B., Malesani, D. B., Palmerio, J. T., et al. 2024, GCN, 38637, 1
Selsing, J., Malesani, D., Goldoni, P., et al. 2019, A&A, 623, A92
Shu, X., Lei, Y., Haonan, Y., et al. 2025, ApJL, 990, L29
Soderberg, A. M., Kulkarni, S. R., Nakar, E., et al. 2006, Natur, 442, 1014
Srinivasaragavan, G. P., Hamidani, H., Schroeder, G., et al. 2025a, ApJL, 988, L60
Srinivasaragavan, G. P., Perley, D. A., Ho, A. Y. Q., et al. 2025b, MNRAS, 538, 351
Srivastav, S., Chen, T. W., Gillanders, J. H., et al. 2025, ApJL, 978, L21
Sun, H., Li, W. X., Liu, L. D., et al. 2025, NatAs, 9, 1073
Svinkin, D., Frederiks, D., Lysenko, A., et al. 2025, GCN, 40167, 1
Tohuvavohu, A., Kennea, J. A., Roberts, C. J., et al. 2024, ApJL, 975, L19
Tsvetkova, A., Frederiks, D., Golenetskii, S., et al. 2017, ApJ, 850, 161
van Dalen, J. N. D., Levan, A. J., Jonker, P. G., et al. 2025, ApJL, 982, L47
van der Horst, A. J., Kouveliotou, C., Gehrels, N., et al. 2009, ApJ, 699, 1087
Vernet, J., Dekker, H., D'Odorico, S., et al. 2011, A&A, 536, A105
Virtanen, P., Gommers, R., Oliphant, T. E., et al. 2020, NatMe, 17, 261
Wanderman, D., & Piran, T. 2010, MNRAS, 406, 1944
Wang, C. Y., Li, A., Zhao, D. H., Li, Z. X. & Einstein Probe Team 2025, GCN, 39329, 1
Wang, Y., Li, D. Y., Zhao, Y. Q., et al. 2025a, GCN, 40257, 1
Wang, Y., Lian, T. Y., Zhang, W. J., et al. 2025b, GCN, 39448, 1
Wang, Y., Sun, H., Wang, Y. L., et al. 2024, GCN, 37034, 1
Wei, J., Cordier, B., Antier, S., et al. 2016, arXiv:1610.06892
Wei, J.-J., & Wu, X.-F. 2025, ApJL, 988, L71
Wijers, R. A. M. J., & Galama, T. J. 1999, ApJ, 523, 177
Woosley, S. E. 1993, ApJ, 405, 273
Woosley, S. E., & Bloom, J. S. 2006, ARA&A, 44, 507
Wu, H. Z., Wang, B. T., Hu, D. F., et al. 2024, GCN, 37997, 1
Wu, Q. Y., Yang, J., Zhou, X. Y., Jin, C. C. & Einstein Probe Team 2025, GCN, 39028, 1
Wu, Q. Y., Zhang, Y. J., Wang, Y., et al. 2024, GCN, 37063, 1
Yadav, M., Troja, E., Ricci, R., et al. 2025, arXiv:2505.08781
Yang, Y.-H., Troja, E., Becerra, R. & ERC BHianca Team 2025a, GCN, 39561, 1
Yang, Y.-H., Troja, E., Becerra, R. & ERC BHianca Team 2025b, GCN, 39574, 1
Yin, Y. H. I., Fang, Y., Zhang, B. B., et al. 2025a, ApJL, 989, L39
Yin, Y. H. I., Hu, J. W., Hua, Y. L., et al. 2025b, GCN, 40085, 1
Yin, Y. H. I., Zhang, B.-B., Yang, J., et al. 2024, ApJL, 975, L27
Yuan, W., Dai, L., Feng, H., et al. 2025, SCPMA, 68, 239501
Yuan, W., Zhang, C., Chen, Y., & Ling, Z. 2022, in Handbook of X-ray and Gamma-ray Astrophysics, ed. C. Bambi & A. Sangangelo (Cham: Springer), 86
Yuan, W., Zhang, C., Feng, H., et al. 2015, arXiv:1506.07735
Zhang, J., Chen, Y., Jia, S., et al. 2025, RAA, 25, 115019

Zhang, W., Yuan, W., Ling, Z., et al. 2025, SCPMA, 68, 219511
Zhang, Y. J., Dai, C. Y., Chen, W., et al. 2025, GCN, 39591, 1
Zhao, X., Ban, H., Cai, H., et al. 2025, ExA, 59, 36
Zheng, J.-H., Zhu, J.-P., Lu, W., & Zhang, B. 2025, ApJ, 985, 21
Zheng, W., Brink, T. G., Filippenko, A. V., et al. 2024a, GCN, 37228, 1
Zheng, W., Brink, T. G., Filippenko, A. V., Yang, Y. & KAIT GRB Team 2024b, GCN, 37959, 1
Zhou, H., Wang, W. X., Hu, J. W., et al. 2024a, GCN, 36997, 1
Zhou, H., Zhao, G. Y., Zhou, C., et al. 2025, GCN, 40165, 1
Zhou, H., Zhu, S. F., Zhang, M. H., et al. 2024b, GCN, 38624, 1
Zhou, H., Zhu, S. F., Zhang, M. H., Jim, C. C. & Einstein Probe team 2024c, GCN, 38606, 1
Zhu, Z. P., Saccardi, A., Schneider, B., et al. 2025a, GCN, 39487, 1
Zhu, Z. P., Schneider, B., Saccardi, A., et al. 2025b, GCN, 39809, 1